Ferromagnetism of a Repulsive Atomic Fermi Gas in an Optical Lattice: A Quantum Monte Carlo Study

S. Pilati
The Abdus Salam International Centre for Theoretical Physics, 34151 Trieste, Italy

I. Zintchenko and M. Troyer
Theoretische Physik, ETH Zurich, 8093 Zurich, Switzerland

(Received 6 August 2013; published 7 January 2014)

Using continuous-space quantum Monte Carlo methods, we investigate the zero-temperature ferromagnetic behavior of a two-component repulsive Fermi gas under the influence of periodic potentials that describe the effect of a simple-cubic optical lattice. Simulations are performed with balanced and with imbalanced components, including the case of a single impurity immersed in a polarized Fermi sea (repulsive polaron). For an intermediate density below half filling, we locate the transitions between the paramagnetic, and the partially and fully ferromagnetic phases. As the intensity of the optical lattice increases, the ferromagnetic instability takes place at weaker interactions, indicating a possible route to observe ferromagnetism in experiments performed with ultracold atoms. We compare our findings with previous predictions based on the standard computational method used in material science, namely density functional theory, and with results based on tight-binding models.

DOI: 10.1103/PhysRevLett.112.015301 PACS numbers: 67.85.-d, 03.75.Hh, 05.30.Fk, 75.20.Ck

Itinerant ferromagnetism, which occurs in transition metals like nickel, cobalt, and iron, is an intriguing quantum mechanical phenomenon due to strong correlations between delocalized electrons. The theoretical tools allowing us to perform *ab initio* simulations of the complex electronic structure of solid state systems, the most important being density functional theory (DFT) [1,2], give systematically reliable results only for simple metals and semiconductors. The extension to strongly correlated materials still represents an outstanding open challenge [3]. Our understanding of quantum magnetism is mostly based on simplified model Hamiltonians designed to capture the essential phenomenology of real materials. The first model introduced to explain itinerant ferromagnetism is the Stoner Hamiltonian [4], which describes a Fermi gas in a continuum with short-range repulsive interactions originally treated at the mean-field level. The Hubbard model, describing electrons hopping between sites of a discrete lattice with on-site repulsion, was also originally introduced to explain itinerant ferromagnetism in transition metals [5]. Despite the simplicity of these models, their zero-temperature ferromagnetic behavior is still uncertain.

In recent years, ultracold atoms have emerged as the ideal experimental system to investigate intriguing quantum phenomena caused by strong correlations. Experimentalists are able to manipulate interparticle interactions and external periodic potentials independently, allowing the realization of model Hamiltonians relevant for condensed matter physics [6], or to test exchange-correlation functionals used in DFT simulations of materials [7]. Indirect evidence consistent with itinerant (Stoner) ferromagnetism was observed in a gas of ^{6}Li atoms [8] when the strength of the repulsive interatomic interaction was increased following the upper branch of a Feshbach resonance. However, subsequent theoretical [9] and experimental studies [10,11] have demonstrated that three-body recombinations are overwhelming in this regime, and an unambiguous experimental proof of ferromagnetic behavior in atomic gases is still missing. Proposed modifications of the experimental setup that should favor the reach of the ferromagnetic instability include: the use of narrow Feshbach resonances [12,13], of mass-imbalanced binary mixtures [14,15], reducing the effective dimensionality with strong confinements [16–19], and adding optical [7] and optical-flux lattices [20].

In this Letter, we use a continuous-space quantum Monte Carlo (QMC) method to investigate ferromagnetism of a 3D two-component Fermi gas with short-range repulsive interspecies interactions in the presence of a simple-cubic optical lattice. At $3/8$ filling (a density of $3/4$ atoms per lattice site) we obtain the zero-temperature phase diagram as a function of interaction strength and the amplitude V_0 of the optical lattice focusing on three phases: paramagnet, partially polarized ferromagnet, and fully polarized ferromagnet. We do not consider spin-textured [21] and antiferromagnetic phases [7,22], nor the Kohn-Luttinger superfluid instability.

Performing simulations in continuous space with an external periodic potential, rather than employing single-band discrete lattice models (valid only in deep lattices), allows us to address also the regime of small V_0 and to determine the shift of the ferromagnetic transition with

respect to the homogeneous gas (corresponding to $V_0 = 0$) [21,23–25]. We consider weak and moderately intense optical lattices, where the noninteracting band-gap is small or zero. We find that the critical interaction strength for the transition between the paramagnetic and the partially ferromagnetic phases (blue circles in Fig. 1), as well as the boundary between the partially and fully polarized ferromagnetic phases (black squares), rapidly decreases when V_0 increases. These results strongly support the idea of observing itinerant ferromagnetism in experiments with repulsive gases in shallow optical lattices [26]. A similar enlargement of the ferromagnetic stability region was obtained by means of DFT simulations based on the Kohn-Sham equations [27] with an exchange-correlation functional obtained within the local spin-density approximation [7,28]. At large lattice depths and interaction strengths, however, we observe quantitative discrepancies between QMC calculations and DFT due to the strong correlations which are only approximately taken into account in DFT methods. This regime, therefore, represents an ideal test bed to develop more accurate exchange-correlation functionals for strongly correlated materials.

This scenario appears to be in contrast with the findings obtained for the single-band Hubbard model, valid for deep lattices and weak interactions, where QMC simulations indicate that the ground-state is paramagnetic [29] (at least up to filling factor $1/4$) and stable ferromagnetism has been found only in the case of infinite on-site repulsion [30–32]. Since at large optical lattice intensity and weak interactions our results agree with Hubbard model simulations (see Supplemental Material [36]), these findings concerning the ferromagnetic transition indicate that the Hubbard model is not an appropriate description for the strongly repulsive Fermi gas in moderately deep optical lattices and that terms beyond on-site repulsion and nearest neighbor hopping play an essential role. It also suggests that the possibility of independently tuning interparticle interactions and spatial inhomogeneity, offered by our continuous-space Hamiltonian, is an important ingredient in explaining itinerant ferromagnetism.

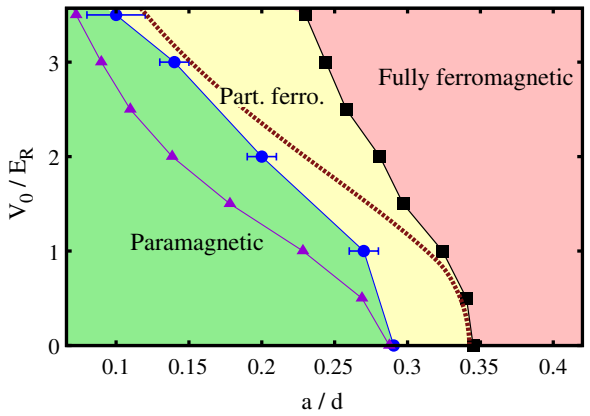

FIG. 1 (color online). Zero-temperature phase diagram at density $nd^3 = 0.75$, as a function of the interactions strength a/d and the optical lattice intensity V_0/E_R. The blue circles separate the region of stability of the paramagnetic phase (green) from the partially polarized ferromagnetic phase (yellow). The black squares separate the partially polarized from the fully polarized ferromagnetic phase (red). The violet triangles and the brown dashed line are the corresponding DFT results. Black and blue lines are guides to the eye.

We investigate the ground-state properties of the Hamiltonian

$$H = \sum_{\sigma=\uparrow,\downarrow} \sum_{i_\sigma=1}^{N_\sigma} [-\Lambda \nabla_{i_\sigma}^2 + V(\mathbf{r}_{i_\sigma})] + \sum_{i_\uparrow, i_\downarrow} v(r_{i_\uparrow i_\downarrow}), \quad (1)$$

where $\Lambda = \hbar^2/2m$, with the atoms' mass m and the reduced Planck constant $\hbar$. The indices $i_\uparrow$ and $i_\downarrow$ label atoms of the two species, which we refer to as spin-up and spin-down fermions, respectively. The total number of fermions is $N = N_\uparrow + N_\downarrow$, and $r_{i_\uparrow i_\downarrow} = |\mathbf{r}_{i_\uparrow} - \mathbf{r}_{i_\downarrow}|$. $V(\mathbf{r}) = V_0 \sum_{\alpha=x,y,z} \sin^2(\alpha\pi/d)$ is a simple-cubic optical lattice potential with periodicity d and intensity V_0, conventionally expressed in units of recoil energy $E_R = \Lambda(\pi/d)^2$. $v(r)$ is a short-range model repulsive potential. Its intensity is parametrized by the s-wave scattering length a, which can be tuned experimentally using Feshbach resonances [33]. Off-resonant intraspecies interactions in dilute atomic clouds are negligible since p-wave collisions are suppressed at low temperature; hence, we do not include them in the Hamiltonian.

We perform simulations of the ground state of the Hamiltonian (1) using the fixed-node diffusion Monte Carlo (DMC) method. The DMC algorithm allows us to sample the lowest-energy wave function by stochastically evolving the Schrödinger equation in imaginary time. To circumvent the sign problem, the fixed-node constraint is imposed, meaning that the many-body nodal surface is fixed to be the same as that of a trial wave function ψ_T. This variational method provides the exact ground-state energy if the exact nodal surface is known, and in general the energies are rigorous upper bounds which are very close to the true ground state if the nodes of ψ_T accurately approximate the ground-state nodal surface (see, e.g., [34,35] and the Supplemental Material [36] for more details). Our trial wave function is of the Jastrow-Slater form

$$\psi_T(\mathbf{R}) = D_\uparrow(N_\uparrow) D_\downarrow(N_\downarrow) \prod_{i_\uparrow, i_\downarrow} f(r_{i_\uparrow i_\downarrow}), \quad (2)$$

where $\mathbf{R} = (\mathbf{r}_1, \ldots, \mathbf{r}_N)$ is the spatial configuration vector and $D_{\uparrow(\downarrow)}$ denotes the Slater determinant of single-particle orbitals of the particles with up (down) spin. The orbitals are constructed by solving the single-particle problem in a box of size L with periodic boundary conditions, with and without an optical lattice, obtaining Bloch wave functions and plane waves, respectively. We employ the $N_{\uparrow(\downarrow)}$

lowest-energy (real-valued) orbitals for the up (down) spins. For homogeneous Fermi gases the accuracy of the Jastrow-Slater form was verified in Ref. [24] by including backflow correlations, and we have performed preliminary simulations with generalized Pfaffian wave functions [37], finding no significative energy reduction. In simulations of the ferromagnetic transition of the infinite-U Hubbard model, fixed-node results were compared against exact released-node simulations [38] finding excellent agreement. Furthermore, at large V_0/E_R and small a/d [where our continuous-space Hamiltonian (1) can be approximated by the Hubbard model] our results precisely agree with those of Ref. [29] (see [36]). These comparisons give us confidence that the choice of ψ_T in (2) accurately estimates the ground-state energy. The Jastrow correlation term $f(r)$ is obtained by solving the two-body scattering problem in free space with the potential $v(r)$ and imposing the boundary condition on its derivative $f\prime(r = L/2) = 0$. With this choice the cusp condition is satisfied. Since $f(r) > 0$, the many-body nodal surface results only from the antisymmetric character of the Slater determinants. We simulate systems of different sizes, up to $L = 6d$ including $N = 162$ fermions, and find that finite-size effects are below statistical error bars if one subtracts the finite-size correction of noninteracting fermions $E_0(N_\uparrow, N_\downarrow) - E_0^{\mathrm{TL}}(P)$, where $E_0^{\mathrm{TL}}(P)$ is the ideal-gas ground-state energy in the thermodynamic limit (TL) at the polarization $P = (N_\uparrow - N_\downarrow)/(N_\uparrow + N_\downarrow)$ [39].

To model the interspecies interaction, we use prevalently the hard-sphere potential (HS): $v(r) = +\infty$ if $r < R_0$ and zero otherwise. At zero temperature, the properties of a dilute homogeneous gas are universal and depend only on the two-body scattering properties at zero energy. These properties are fixed by the s-wave scattering length a. For the HS model, one has $a = R_0$. As a increases, other details of the potential might become relevant, the most important being the effective range r_{eff} and the p-wave scattering length a_p [40], which characterize scattering at low but finite energy [41]. For homogeneous systems, a detailed analysis of the nonuniversal effects was performed in Refs. [23–25]. Various models with different values of r_{eff} and a_p were considered, including resonant attractive potentials designed to mimic broad Feshbach resonances with $r_{\mathrm{eff}} \ll n^{-1/3}$ ($n = N/L^3$ is the density) [33]. In this Letter, we consider the limited interaction regime $k_F a \lesssim 1$ [$k_F = (3\pi^2 n)^{1/3}$ is the Fermi wave vector], where differences in the equations of state were found to be marginal (see Fig. 2, lower dataset). In the presence of an optical lattice, the single-particle band structure further complicates the two-body scattering process. To analyze nonuniversal effects in this situation, we compare the many-body ground-state energies in optical lattices obtained using three model potentials with the same s-wave scattering length: the HS model; the soft-sphere potential (SS), $v(r) = v_{\mathrm{SS}}$ if $r < R_0$ and zero otherwise, with $R_0 = 2a$ [42]; the negative-power potential (NP) $v(r) = v_{\mathrm{NP}}/r^9$ [43]. In Fig. 2 (upper dataset), we show results for an optical lattice with intensity $V_0 = 3E_R$. Nonuniversal corrections are found to be below statistical error-bars up to values of the interaction parameter where ferromagnetic behavior occurs (see below). In the following, we use the HS model and parametrize the interaction strength with the parameters $k_F a$ and a/d, in free space and in optical lattices, respectively. The latter can be compared with the former if one defines k_F with the average density in the optical lattice.

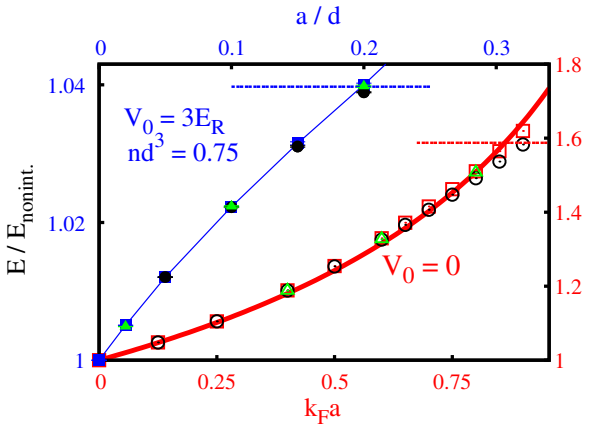

FIG. 2 (color online). Ground-state energy in an optical lattice (upper dataset with full symbols, left and upper blue axes) and in free space (empty symbols, lower and right red axes). Three interatomic potentials are considered: hard spheres (HS, blue and red squares), soft spheres (SS, black circles), and negative power (NP, green triangles). The ranges of interaction strength in the upper and lower x axes coincide if one defines $k_F = (3\pi^2 n)^{1/3}$ with the average density n in the optical lattice. The horizontal segments indicate the energies of the fully polarized phases. The thick red curve is the ladder approximation theory for a zero-range pseudopotential [25].

Many theoretical studies of atomic gases in optical lattices have instead adopted discrete lattice models within a single-band approximation and with on-site interactions only. The on-site interaction parameter is usually determined without considering the strong virtual excitations to higher Bloch bands which are induced by short-ranged potentials [45]. This approximation is reliable only if $V_0 \gg E_R$ and $a \ll d$ [46]. In the regime considered in this Letter, higher-band processes are important and they can have a strong impact on the properties of discrete-lattice models [47]. Reference [45] introduced a different procedure to determine the on-site Hubbard interaction parameter which is valid at low filling and effectively takes into account the role of higher bands.

To determine the onset of ferromagnetism using QMC calculations, we perform simulations of population-imbalanced configurations. In Fig. 3, we plot the energy as a function of polarization P for fixed lattice depth $V_0 = 2E_R$ and density $nd^3 = 0.75$ at different interaction strengths. The minimum of the curve $E(P)$ indicates

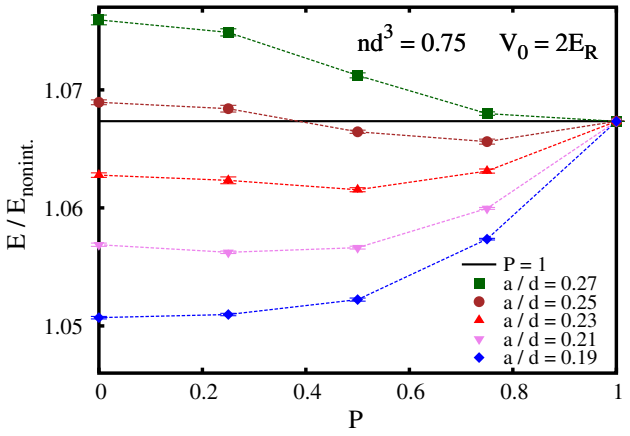

FIG. 3 (color online). Energy versus population imbalance $P = (N_\uparrow - N_\downarrow)/(N_\uparrow + N_\downarrow)$ for the different values of interaction strength a/d. The horizontal black line is the energy of the fully polarized gas, dashed lines are a guide to the eye.

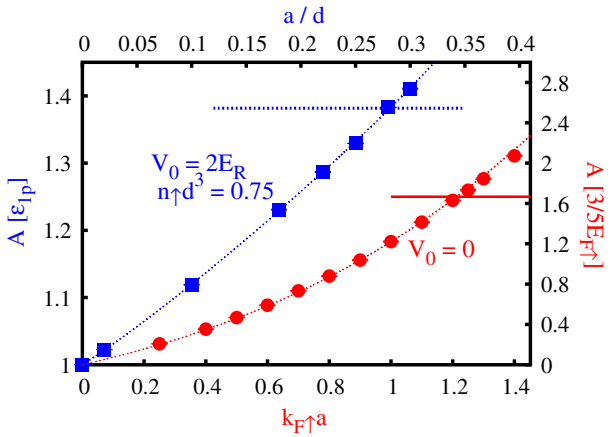

FIG. 4 (color online). Chemical potential at zero concentration of the repulsive polaron in an optical lattice (blue squares, left and upper axes) and in free space (red circles, right and bottom axes). ϵ_{1p} is the energy at the bottom of the noninteracting Bloch band, $E_{F\uparrow} = \hbar^2 k_{F\uparrow}^2/2m$. The ranges of interaction strength in the upper and lower x axes coincide if one defines $k_{F\uparrow} = (6\pi^2 n)^{1/3}$ with the average density n in the optical lattice. The horizontal segments indicate the chemical potential of the majority component.

the equilibrium polarization of ferromagnetic domains. At the weakest interaction, the minimum is at $P = 0$, so the system is paramagnetic. For larger a/d, we observe minima at finite P, allowing us to estimate the critical interaction strength where the transition to the partially ferromagnetic phase takes place. We do not investigate here the order of the transition. Our results are compatible with different scenarios which have been proposed: weakly first-order [48], second-order [25], or infinite-order [38] transitions. A similar analysis at different optical lattice intensities shows that the critical interaction strength rapidly diminishes as V_0 increases (see blue bullets in Fig. 1), meaning that the optical lattice strongly favors ferromagnetism.

The critical interaction strength between the partially and the fully polarized phases is found by considering the problem of the repulsive Fermi polaron, i.e., a single impurity, say a spin-down particle, immersed in a fully polarized gas of spin-up particles. In Fig. 4, we show the polaron chemical potential A, i.e., the energy of the gas with the impurity minus the energy of the spin-up particles alone, as a function of the interaction strength. We compare results obtained in a $V_0 = 2E_R$ optical lattice (blue squares), with the homogeneous case $V_0 = 0$ (red circles, from Ref. [23]). In the region where A is larger than the chemical potential of the majority component (horizontal segments in Fig. 4), the fully polarized phase is stable. By repeating a similar analysis for different values of V_0, the phase boundary between the two phases (black squares in Fig. 1) is obtained.

In conclusion, we have calculated, using QMC methods, the ground-state energy of repulsive Fermi gases in optical lattices as a function of population imbalance, obtaining the critical interaction strength for the onset of ferromagnetic behavior. From simulations of the repulsive polaron, we determined the region of stability of the fully polarized phase. Of particular interest is the question of how effective strongly correlated single-band models emerge from the continuum description. In the context of the Mott insulator transition in bosonic systems, lattice models with only on-site interaction have been compared against continuous-space simulations, finding for $V_0 \gtrsim 4E_R$ only quantitative differences [49]. However, in the regime of intermediate values of V_0 and strong interactions considered in this Letter, additional terms such as density-induced tunneling and interaction-induced higher band processes are important, and they can induce qualitative changes in the properties of tight binding models [47,50,51], in particular, concerning the ferromagnetic behavior [52]. These effects are naturally taken into account in a continuous-space description, and our results confirm that they play a role in itinerant ferromagnets.

While in shallow lattices there is good agreement between QMC and Kohn-Sham local spin-density approximation, the regime of deep lattices and strong interactions represents a new test bed to develop more accurate exchange-correlation functionals, which is an outstanding open challenge in material science [3]. Furthermore, our results show that moderately intense optical lattices are favorable for experimental realization of ferromagnetism, also due to a faster thermalization rate compared to very deep lattices. In a recent experiment short-range antiferromagnetic correlations have been observed at half-filling [53].

We thank Lianyi He for providing us data from Ref. [25], Chia-Chen Chang for the data from Ref. [29], M. Capone, F. Becca, Lei Wang, and N. Prokof'ev for useful

discussions. This work was supported by ERC Advanced Grant No. SIMCOFE, the Swiss National Competence Center in Research QSIT, and the Aspen Center for Physics under Grant No. NSF 1066293.

[1] W. Kohn, A. D. Becke, and R. G. Parr, J. Phys. Chem. **100**, 12974 (1996).
[2] P. Hohenberg and W. Kohn, Phys. Rev. **136**, B864 (1964).
[3] A. J. Cohen, P. Mori-Sánchez, and W. Yang, Chem. Rev. **112**, 289 (2012).
[4] E. Stoner, Philos. Mag. **15**, 1081 (1933).
[5] J. Hubbard, Proc. R. Soc. A **276**, 238 (1963).
[6] D. Jaksch and P. Zoller, Ann. Phys. (Amsterdam) **315**, 52 (2005).
[7] P. N. Ma, S. Pilati, M. Troyer, and X. Dai, Nat. Phys. **8**, 601 (2012).
[8] G.-B. Jo, Y.-R. Lee, J.-H. Choi, C. A. Christensen, T. H. Kim, J. H. Thywissen, D. E. Pritchard, and W. Ketterle, Science **325**, 1521 (2009).
[9] D. Pekker, M. Babadi, R. Sensarma, N. Zinner, L. Pollet, M. W. Zwierlein, and E. Demler, Phys. Rev. Lett. **106**, 050402 (2011).
[10] Y.-R. Lee, M.-S. Heo, J.-H. Choi, T. T. Wang, C. A. Christensen, T. M. Rvachov, and W. Ketterle, Phys. Rev. A **85**, 063615 (2012).
[11] C. Sanner, E. J. Su, W. Huang, A. Keshet, J. Gillen, and W. Ketterle, Phys. Rev. Lett. **108**, 240404 (2012).
[12] C. Kohstall, M. Zaccanti, M. Jag, A. Trenkwalder, P. Massignan, G. M. Bruun, F. Schreck, and R. Grimm, Nature (London) **485**, 615 (2012).
[13] P. Massignan, Z. Yu, and G. M. Bruun, Phys. Rev. Lett. **110**, 230401 (2013).
[14] C. W. von Keyserlingk and G. J. Conduit, Phys. Rev. A **83**, 053625 (2011).
[15] X. Cui and T.-L. Ho, Phys. Rev. Lett. **110**, 165302 (2013).
[16] F. Serwane, G. Zurn, T. Lompe, T. B. Ottenstein, A. N. Wenz, and S. Jochim, Science **332**, 336 (2011).
[17] S. E. Gharashi and D. Blume, Phys. Rev. Lett. **111**, 045302 (2013).
[18] E. J. Lindgren *et al.*, arXiv:1304.2992.
[19] P. O. Bugnion and G. J. Conduit, Phys. Rev. A **87**, 060502 (2013).
[20] S. K. Baur and N. R. Cooper, Phys. Rev. Lett. **109**, 265301 (2012).
[21] G. J. Conduit, A. G. Green, and B. D. Simons, Phys. Rev. Lett. **103**, 207201 (2009).
[22] C. J. M Mathy and D. A. Huse, Phys. Rev. A **79**, 063412 (2009).
[23] S. Pilati, G. Bertaina, S. Giorgini, and M. Troyer, Phys. Rev. Lett. **105**, 030405 (2010).
[24] S.-Y. Chang, M. Randeria, and N. Trivedi, Proc. Natl. Acad. Sci. U.S.A. **108**, 51 (2011).
[25] L. He and X.-G. Huang, Phys. Rev. A **85**, 043624 (2012).
[26] I. Zintchenko, L. Wang, and M. Troyer, arXiv:1308.1961.
[27] W. Kohn and L. J. Sham, Phys. Rev. **140**, A1133 (1965).
[28] We improved the DFT simulations of Ref. [7] using 101^3 k points.
[29] C.-C. Chang, S. Zhang, and D. M. Ceperley, Phys. Rev. A **82**, 061603(R) (2010).
[30] F. Becca and S. Sorella, Phys. Rev. Lett. **86**, 3396 (2001).
[31] H. Park, K. Haule, C. A. Marianetti, and G. Kotliar, Phys. Rev. B **77**, 035107 (2008).
[32] L. Liu, H. Yao, E. Berg, S. R. White, and S. A. Kivelson, Phys. Rev. Lett. **108**, 126406 (2012).
[33] C. Chin, R. Grimm, P. Julienne, and E. Tiesinga, Rev. Mod. Phys. **82**, 1225 (2010).
[34] P. J. Reynolds, D. M. Ceperley, B. J. Alder, and W. A. Lester, Jr., J. Chem. Phys. **77**, 5593 (1982).
[35] W. M. C Foulkes, L. Mitas, R. J. Needs, and G. Rajagopal, Rev. Mod. Phys. **73**, 33 (2001).
[36] See Supplemental Material at http://link.aps.org/supplemental/10.1103/PhysRevLett.112.015301 for more details on the computational method and a comparison with Hubbard model results.
[37] M. Bajdich, L. Mitas, L. K. Wagner, and K. E. Schmidt, Phys. Rev. B **77**, 115112 (2008).
[38] G. Carleo, S. Moroni, F. Becca, and S. Baroni, Phys. Rev. B **83**, 060411 (2011).
[39] C. Lin, F. H. Zong, and D. M. Ceperley, Phys. Rev. E **64**, 016702 (2001).
[40] R. F. Bishop, Ann. Phys. (N.Y.) **77**, 106 (1973).
[41] The s-wave and p-wave scattering phase shifts satisfy the relations $k \cot[\delta_0(k)] = -1/a + r_{\rm eff}k^2/2 + o(k^4)$ and $k^3 \cot[\delta_1(k)] = -3/a_p^3 + o(k^2)$, where k is the scattering wave vector. For the HS model, one has $r_{\rm eff} = 2a/3$ and $a_p = a$.
[42] For the SS potential: $a = R_0[1 - \tanh(K_0)/K_0]$, with $K_0^2 = v_{\rm SS}R_0^2/(2\Lambda)$; $r_{\rm eff} = R_0 - R_0^3/(3a^2) + 1/(K_0^2 a) \simeq 0.41a$; $a_p = R_0\{1 - 3[1 - K_0\coth(K_0)]/K_0^2\}^{1/3} \simeq 1.13a$.
[43] For the NP potential: $a \cong 0.678(v_{\rm NP}m/\hbar^2)^{1/7}$. We determine $r_{\rm eff} \cong 0.63a$ and $a_p \cong 1.29a$ by solving numerically the integral equation given in Ref. [44].
[44] L. P. Benofy, E. Buendia, R. Guardiola, and M. de Llano, Phys. Rev. A **33**, 3749 (1986).
[45] H. P. Büchler, Phys. Rev. Lett. **104**, 090402 (2010); Phys. Rev. Lett. **108**, 069903(E) (2012).
[46] D. Jaksch, C. Bruder, J. I. Cirac, C. W. Gardiner, and P. Zoller, Phys. Rev. Lett. **81**, 3108 (1998).
[47] D. S. Luehmann, O. Juergensen, and K. Sengstock, New J. Phys. **14**, 033021 (2012).
[48] D. Belitz, T. R. Kirkpatrick, and T. Vojta, Phys. Rev. Lett. **82**, 4707 (1999).
[49] S. Pilati and M. Troyer, Phys. Rev. Lett. **108**, 155301 (2012).
[50] A. Mering and M. Fleischhauer, Phys. Rev. A **83**, 063630 (2011).
[51] A. A. Aligia, A. Anfossi, L. Arrachea, C. D. E. Boschi, A. Dobry, C. Gazza, A. Montorsi, F. Ortolani, and M. Torio, Phys. Rev. Lett. **99**, 206401 (2007).
[52] J. C. Amadon and J. E. Hirsch, Phys. Rev. B **54**, 6364 (1996).
[53] D. Greif, T. Uehlinger, G. Jotzu, L. Tarruell, and T. Esslinger, Science **340**, 1307 (2013).